

Low-temperature crystal and magnetic structures of the chain-ladder composite material $\text{Sr}_{0.4}\text{Ca}_{13.6}\text{Cu}_{24+y}\text{O}_{41+z}$: Hole redistribution and antiferromagnetic order

M. Isobe, M. Onoda, T. Ohta, F. Izumi, K. Kimoto, and E. Takayama-Muromachi
National Institute for Research in Inorganic Materials (NIRIM), 1-1 Namiki, Tsukuba, Ibaraki 305-0044, Japan

A. W. Hewat
Institut Max von Laue-Paul Langevin (ILL), BP 156, F-38042 Grenoble Cedex 9, France

K. Ohoyama
Institute for Materials Research (IMR), Tohoku University, Sendai 980-8577, Japan
 (Received 1 May 2000)

The low-temperature crystal structure of a one-dimensional chain-ladder composite material $\text{Sr}_{0.4}\text{Ca}_{13.6}\text{Cu}_{24+y}\text{O}_{41+z}$ was determined by the Rietveld analysis of neutron diffraction data using a superspace group approach. The hole distribution between the chain and ladder planes was estimated by the bond-valence sum (BVS) calculation based on Cu-O interatomic distances. The minimum of the distance between ladder-copper and chain-oxygen atoms [Cu(1)-O(3)] was revealed to expand with lowering temperature. The BVS calculation indicated that such a structural change corresponds to a redistribution of holes from the ladder to the chain and that almost all of the holes are localized in the chain below or near the Néel temperature. By assuming reasonable magnetic interactions between hole-unoccupied Cu sites on the chain plane, we propose a possible magnetic structure model taking into account the distribution of holes and observed magnetic neutron Bragg reflections. The results suggest the presence of spin dimers, spin trimers, and ‘‘lone’’ spins in the chain, of which the latter two have effective magnetic moments. These moments may be an origin of staggered antiferromagnetic spin modulation onto the spin-liquid state.

I. INTRODUCTION

The one-dimensional chain-ladder composite material $\text{Sr}_{14-x}\text{Ca}_x\text{Cu}_{24+y}\text{O}_{41+z}$ shows two striking quantum phenomena at low temperature. One is the formation of hole pairs realized in a spin-liquid ground state in the ladder,^{1,2} and the other is antiferromagnetic long-range order coexisting with spin singlets.^{3,4} These phenomena seem to be crucial for understanding the mechanism of superconductivity in the spin-ladder system as well as in high- T_C cuprates.

The formal valence of Cu in this compound is nearly +2.25; namely, about six holes per formula unit are ‘‘self-doped’’ in the system. The distribution of the holes is one of the most important factors that govern the physical properties of the system. It has been reported that most holes are located in the chain in the Ca-free phase with $x=0$, but some of them are transferred into the ladder as the Ca content increases.^{5,6} Associated with the hole transfer, electric conductivity increases with the Ca content, but it remains semiconductorlike in a low-temperature region even in the Ca-richest sample with $x=13.6$. Under high pressure, the hole transfer into the ladder is further enhanced in accordance with a shortening of a ladder-chain interplane distance.⁷ An insulator-to-metal transition is induced by pressure in the highly Ca-doped phase, and finally, superconductivity appears at low temperature.⁸

Antiferromagnetic long-range order has been observed at ambient pressure in highly Ca-doped samples with a Néel temperature (T_N) below the liquid-He temperature.³ The antiferromagnetism is no doubt related to the ‘‘self-doped’’

holes and their localization at low temperature. A localized hole is expected to destroy a spin singlet, yielding a ‘‘lone’’ spin, which induces staggered spin modulation on the remaining spin-singlets.^{3,9,10} This is a possible scenario of the antiferromagnetic long-range order in the spin-liquid state, but there is no definite experimental evidence to support this picture for the present system. Therefore, the determination of the hole distribution at low temperature is indispensable for understanding the origin of the antiferromagnetism.

In the present composite system, modulation of the crystal structure strongly affects the distribution of the localized holes. However, details of the low-temperature crystal structure have not been known because the conventional structure refinement cannot be applied for the present incommensurately modulated structure.

In this paper, we determine the crystal structure of $\text{Sr}_{0.4}\text{Ca}_{13.6}\text{Cu}_{24+y}\text{O}_{41+z}$ by the Rietveld analysis of neutron powder diffraction data measured at low temperature under ambient pressure. Structural parameters were refined using a technique on the basis of a four-dimensional description of the modulated structure, which enables us to extract maximum structural information from the powder diffraction data. The distribution of holes between the chain and ladder was determined by the bond-valence sum (BVS) calculation using Cu-O interatomic distances refined.¹¹ We compared the low-temperature crystal structure with the room-temperature one¹² from the viewpoint of the redistribution of holes between the chain and ladder, and found that holes located in the ladder at 300 K tend to move into the chain with lowering temperature. We concluded that almost all of the holes are localized in the chain near or below T_N . Fur-

thermore, on the basis of the hole distribution obtained by the BVS calculation and reasonable spin-spin interactions on the chain Cu sites, we proposed a possible magnetic structure model that is consistent with experimental magnetic scattering intensities. We discuss the origin of the antiferromagnetic long-range order based on the magnetic structure model.

II. EXPERIMENT

A pure polycrystalline sample of $\text{Sr}_{0.4}\text{Ca}_{13.6}\text{Cu}_{24+y}\text{O}_{41+z}$ was prepared by means of the conventional solid-state reaction using an O_2 -hot-isostatic-press technique.⁷ The sample was confirmed to show an antiferromagnetic transition at $T_N=3.6$ K by static magnetic measurements.¹³

Neutron powder diffraction data for crystal-structure analysis were collected at 1 h per scan at 5 K using a cryostat on the high-resolution powder diffractometer D2B at ILL in the high-intensity mode.¹⁴ The white beam of neutrons from the high-flux reactor was monochromized to a wavelength of 1.5949 Å with a composite focusing Ge monochromator.

Neutron powder diffraction experiments for observation of magnetic reflections were carried out on the HERMES powder diffractometer of IMR installed at the T1-3 beam line in the guide hall at the JRR-3M reactor of the Japan Atomic Energy Research Institute (JAERI).¹⁵ The incident neutron beam with a wavelength of 1.8196 Å was obtained with the 331 reflection of a bent-crystalline Ge monochromator and 12'-open-sample-22' collimation. The powder sample was put into a cylindrical vanadium cell with a diameter of 10 mm and mounted in a cryostat with liquid He. The diffraction data were collected at 1.5 and 5 K in a 2θ range from 2° to 152° in a step size of 0.1°.

Electron diffraction patterns were taken at 107 K from crushed particles on a liquid- N_2 -type cold stage on a high-resolution transmission electron microscope (Hitachi H-1500) operated at 800 kV.¹⁶

III. STRUCTURE ANALYSIS

Figure 1 shows a structure drawing of $\text{Sr}_{0.4}\text{Ca}_{13.6}\text{Cu}_{24+y}\text{O}_{41+z}$. It is a composite crystal which consists of two interpenetrated subsystems with different c -axis lengths: c_1 and c_2 . The first subsystem includes Cu_2O_3 corner-sharing two-leg ladders, while the second subsystem has CuO_2 edge-sharing one-dimensional chains running in the same direction.¹⁷ The $c_1:c_2$ is nearly $\sqrt{2}:1$. Its atomic positions are incommensurately modulated owing to the interaction between the two subsystems.

Figures 2(a) and 2(b) are electron diffraction patterns observed at 107 K on a^*-b^* and b^*-c^* sections, respectively. These patterns are essentially identical to those observed at 300 K,⁷ which show the absence of a structural phase transition at least down to 107 K. This result is consistent with a low-temperature x-ray diffraction study.⁷ The main reflections are assigned by the superimposition of two sets of orthorhombic reciprocal lattices corresponding to the two subsystems. The real lattices of the two subsystems have common a and b dimensions ($a \approx 11.26$ Å and $b \approx 12.38$ Å) but different c dimensions ($c_1 \approx 3.90$ Å and $c_2 \approx 2.74$ Å). Along the c^* direction, we observed some satellite spots due

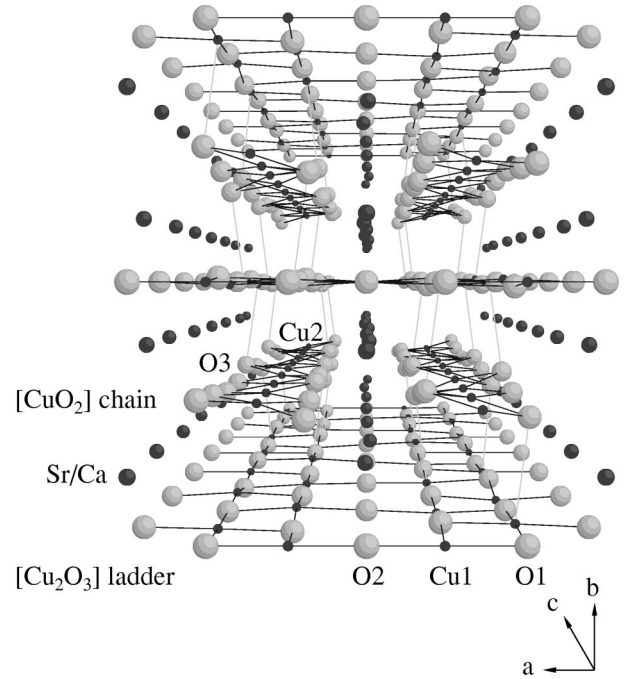


FIG. 1. Modulated structure of a composite crystal $\text{Sr}_{0.4}\text{Ca}_{13.6}\text{Cu}_{24+y}\text{O}_{41+z}$ at 5 K projected along the $[001]$ direction. The intrasubsystem Cu-O bonds are drawn by black solid lines, while the intersubsystem Cu-O bonds with $l \leq 2.85$ Å are drawn by gray solid lines.

to incommensurate modulation resulting from the interaction between the two subsystems. Both the main and satellite reflections are systematically indexed by a set of four integers $hk\ell m$, with a reciprocal-lattice vector \mathbf{q} given by

$$\mathbf{q} = h\mathbf{a}^* + k\mathbf{b}^* + \ell\mathbf{c}_1^* + m\mathbf{c}_2^* \quad (\text{Ref. } 18).$$

Reflection conditions for the fundamental spots with $\ell=0$ and/or $m=0$ are $h+k=2n$, $k+l=2n$, and $l+h=2n$ for $hk\ell 0$ and $h+k=2n$, $k+m=2n$, and $m+h=2n$ for $hk0m$, which reveals that each subsystem has a face-centered lattice. Possible space groups of the basic structures for the two subsystems are, therefore, $Fmmm$, $F222$, $F2mm$, $Fm2m$, and $Fmm2$. To determine the superspace group of a composite crystal, we have to know the space groups of two basic subsystems. In the present case, 25 possibilities were considered first as the combination of the basic space groups. After preliminary studies of the superspace groups, five combinations $Fmmm$ - $Fmmm$, $F222$ - $F222$, $F2mm$ - $F2mm$, $Fm2m$ - $Fm2m$, and $Fmm2$ - $Fmm2$ were selected, and then we finally adopted $F222$ - $F222$ on the basis of structure refinements with the most probable basic space groups. The corresponding superspace group is denoted as $F222(11\gamma):F222(11\gamma)$, which is the same superspace group as that used in the analysis of the room-temperature structure¹² and equivalent to $F222(00\gamma)$ (No. 22.1) in Table 9.8.3.5 in Ref. 19. Symmetry operations of the superspace group are summarized in Table I.

The diffraction data measured on D2B were analyzed with a Rietveld-refinement program PREMOS,²⁰ based on the above superspace group. Initial structural parameters of the fundamental structure were taken from the previous paper¹² and are listed in Table II. The occupation factors g of Sr and

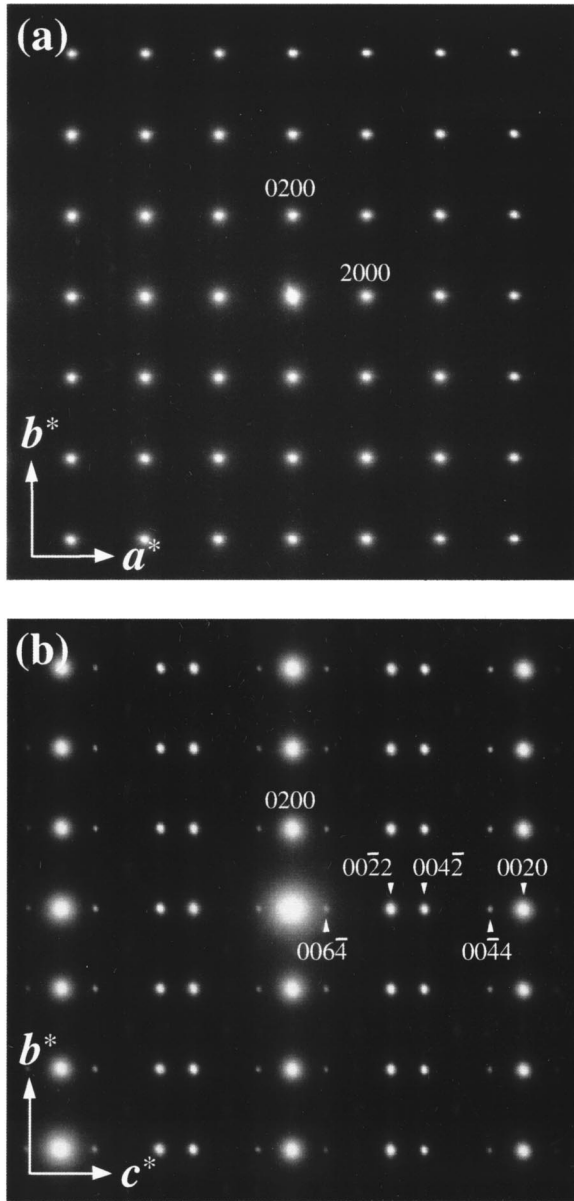


FIG. 2. Electron diffraction patterns of $\text{Sr}_{0.4}\text{Ca}_{13.6}\text{Cu}_{24+y}\text{O}_{41+z}$ observed at 107 K on a^*-b^* (a) and b^*-c^* (b) sections.

Ca at the Sr/Ca site were, respectively, fixed at 0.029 and 0.971 on the assumption of their random distribution. The occupancies of the other atoms were fixed at unity. Isotropic atomic displacement parameters B were assigned for all sites. The preferred orientation due to a needlelike crystal habit was corrected with a preferred-orientation vector of \mathbf{b}^* . The

2θ range used in the analysis was from 10° to 158° , which corresponds to the lattice-plane spacing d from 9.15 to 0.81 Å. Bound coherent scattering lengths for Sr, Ca, Cu, and O were taken from Ref. 21.

For a modulated subsystem, deviations from fundamental structural parameters can be described by the following modulation function in terms of Fourier series:

$$c(t) = A_0 + \sum_{n=0}^m [A_n \cos(2\pi nt) + B_n \sin(2\pi nt)],$$

where c is one of displacement modulations u , v , w , or the modulation in the B parameter. Here t is the fourth-dimension coordinate of the fundamental structure.^{22,23} In the present analysis, the maximum order of harmonics, m , was set at 2 in the displacement modulations u , v , and w , for all sites. Although there are satellite spots with the order higher than second, e.g., $00\bar{4}4$ and $006\bar{4}$, in the electron diffraction patterns, they were weak and were not observed in the neutron powder pattern. Only the constant term A_0 was considered in the B parameters for all sites, i.e., $A_{i=1,2} = B_{i=1,2} = 0$ for B . For the sites with a special position in the super-space group, all of the Fourier coefficients are not variable. The coefficients denoted by the symbol “-” in Table II are zero because of such constraints. As a result, the x , y positions for O(2) and Cu(2) sites were fixed at their initial values. The total number of structural parameters refined in the analysis was 38, including 32 Fourier amplitudes in the modulation functions for fractional coordinates and 6 B parameters.

IV. RESULTS AND DISCUSSION

A. Crystal structure at 5 K

The refinement was completed with $R_{\text{wp}} = 6.71\%$. Table II lists the resulting structural parameters, and Fig. 3 represents calculated, observed, and difference patterns for the neutron powder diffraction data. The crystal structure at 5 K is illustrated in Fig. 1. Comparison of the lattice parameters at 5 K listed in Table III with those at 300 K (Ref. 12) shows that lattice shrinkage is anisotropic with 0.038%, 0.36%, and 0.091% for the a , b , and c axes, respectively. These values agree well with those observed in a previous x-ray study.⁷

B. Hole redistribution with lowering temperature

Figure 4 shows interatomic distances between Cu(1) (ladder) or Cu(2) (chain) and O atoms at 5 K plotted as the function of a fourth coordinate t' , which represents the dis-

TABLE I. Assumed four-dimensional space group symmetry for $\text{Sr}_{0.4}\text{Ca}_{13.6}\text{Cu}_{24+y}\text{O}_{41+z}$.

Subsystem	1: $[(\text{Sr}, \text{Ca})_2\text{Cu}_2\text{O}_3]_\infty$	2: $[\text{CuO}_2]_\infty$
Modulation vector \mathbf{k}	$(c_1/c_2)\mathbf{c}_1^*$	$(c_2/c_1)\mathbf{c}_2^*$
Generators	$x, y + 1/2, z + 1/2, t + 1/2$ $x + 1/2, y, z + 1/2, t + 1/2$ $x, -y, -z, -t$ $-x, y, -z, -t$	$x, y + 1/2, z + 1/2, t + 1/2$ $x + 1/2, y, z + 1/2, t + 1/2$ $x, -y, -z, -t$ $-x, y, -z, -t$
Symbol	$F222(11\gamma)$	$F222(11\gamma)$

TABLE II. Fractional coordinates x , y , and z and isotropic atomic displacement parameters B of each atom for the fundamental structure and modulated one obtained by neutron Rietveld refinement of $\text{Sr}_{0.4}\text{Ca}_{13.6}\text{Cu}_{23.981}\text{O}_{40.963}$. The A_i and B_i ($i \leq 2$) are the Fourier amplitude in the modulation function. Numbers in parentheses are estimated standard deviations of the last significant digit.

Atom	Site		x	y	z	B (\AA^2)
Subsystem 1: $[(\text{Sr}, \text{Ca})_2\text{Cu}_2\text{O}_3]_\infty$						
Sr/Ca	8e	Fundamental	0.0	0.131	0.0	1.0
		A_0		-0.0016(3)		-0.59(9)
		A_1		0.000(3)		0 ^a
		B_1	0.005(1)		0.019(6)	
		A_2		0.001(2)		0 ^a
Cu(1)	8f	Fundamental	0.334	0.0	0.0	1.0
		A_0	0.0000(2)			-0.91(7)
		A_1	0.003(2)			0 ^a
		B_1		-0.069(7)	0.018(4)	
		A_2	-0.001(1)			0 ^a
O(1)	8f	Fundamental	0.167	0.0	0.0	1.0
		A_0	-0.0014(3)			-0.75(8)
		A_1	-0.001(3)			0 ^a
		B_1		-0.0069(9)	0.002(6)	
		A_2	-0.001(2)			0 ^a
O(2)	4b	Fundamental	0	0	0.5	1.0
		A_0				-0.45(9)
		A_1				0 ^a
		B_1			0.00(1)	
		A_2				0 ^a
		B_2			-0.008(4)	
Subsystem 2: $[\text{CuO}_2]_\infty$						
Cu(2)	4c	Fundamental	1/4	1/4	0.25	1.0
		A_0				-0.48(7)
		A_1			0.057(5)	
		B_1				0 ^a
		A_2				0 ^a
O(3)	8i	Fundamental	0.25	0.636	0.25	1.0
		A_0	-0.0014(3)			-0.19(8)
		A_1		-0.0233(6)	-0.024(6)	
		B_1	-0.002(2)			0 ^a
		A_2	-0.0023(8)			0 ^a
		B_2		-0.010(2)	0.025(3)	

^aFixed in the Rietveld refinement.

tance from three-dimensional space. Cu(1)-O(1), Cu(1)-O(2), and Cu(2)-O(3) distances are intraplane ones, while Cu(1)-O(3) and Cu(2)-O(1) distances are interplane ones. The variations of the intraplane distances show that displacement modulations are more pronounced in the chain than in the ladder. As seen in Fig. 1, the most remarkable structural feature in this system is the extreme tilt of the Cu(2)-O(3) chain around the c axis. As a result of such a tilt, parts of O(3) atoms are displaced considerably and approach Cu(1) atoms of the neighboring ladders as apical oxygen atoms. The parts of Cu(1) atoms in the ladder are, therefore, coordinated to the O(3) atoms, forming CuO_5 tetragonal pyramids.

Figure 5 shows those Cu-O distance waves obtained at 300 K, which are cited from Ref. 12. The overall feature of the structure does not change significantly between 5 and 300 K, but marked differences are noticed if we compare Figs. 4 and 5 in more details. In particular, the minimum Cu(1)-O(3) distance increased from 2.661 to 2.740 \AA as the temperature is lowered from 300 to 5 K. On the contrary, the average Cu(1)-O(3) distance is shortened by 0.67% from 2.896 \AA at 300 K to 2.877 \AA at 5 K. Here the average value was calculated by averaging distances between Cu(1) and its nearest O(3) atoms. The average shortening of 0.67% is comparable to the b -axis shrinkage of 0.36% and seems to be mainly attributed to the thermal contraction of the lattice.

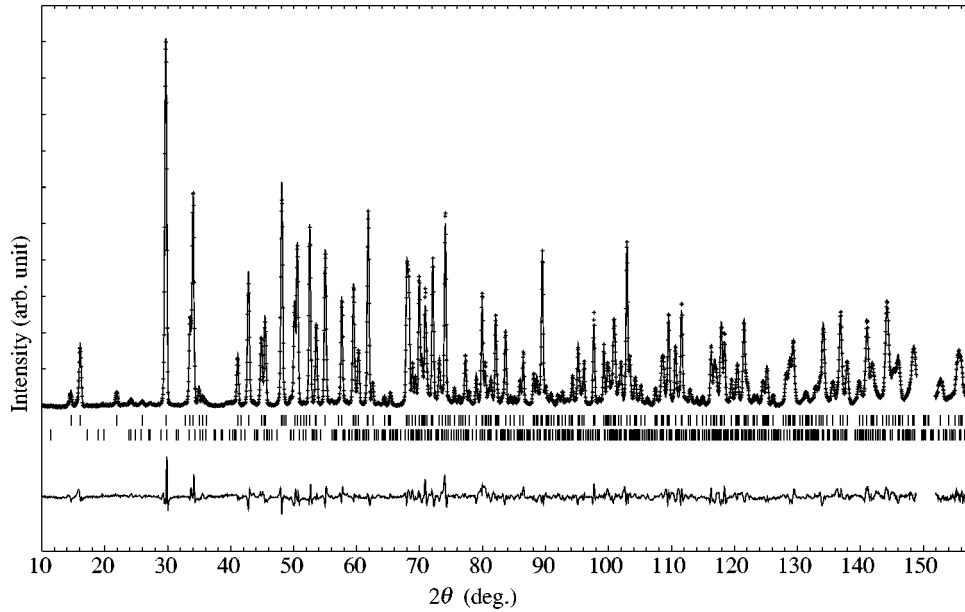


FIG. 3. Rietveld-refinement pattern for the neutron diffraction data at 5 K of $\text{Sr}_{0.4}\text{Ca}_{13.6}\text{Cu}_{23.981}\text{O}_{40.963}$. The cross symbols indicate observed intensities, and the solid line on them is the calculated pattern. Short vertical lines below the profile indicate the peak positions of main (upper) and satellite (lower) reflections. The lowest pattern indicates the difference between the observed and calculated intensities. The resultant reliability factor R_{wp} was 6.71%.

Associated with the change in the Cu(1)-O(3) distance wave, amplitudes, and phases of the three Cu(1)-O(1) distance waves also change slightly with lowering temperature.

For a pyramidal Cu(1) atom with a short Cu(1)-O(3) distance, the intraplane Cu(1)-O(1) and Cu(1)-O(2) distances are also shortened markedly. This supports the idea that holes preferably enter the sites having short Cu(1)-O(3) distances.¹² Because most ‘‘self-doped’’ holes are located in the chain and the hole density in the ladder is one per formula unit at most,²⁴ the minimum Cu(1)-O(3) distance is a more important factor governing the hole density in the ladder than the averaged one. The structural changes described above, therefore, indicate that the hole density in the ladder tends to decrease with lowering temperature. This point is discussed below on the basis of the BVS calculation.

Figure 6 shows BVS waves of the Cu(1) sites (a) and Cu(2) sites (b) in $\text{Sr}_{0.4}\text{Ca}_{13.6}\text{Cu}_{24+y}\text{O}_{41+z}$ at 5 and 300 K plotted against the four-dimensional coordinate t' . The BVS is an empirical measure of the oxidation state for a cation; in

the present case, it corresponds to a probability of the presence of a hole at each Cu site. An apparent change is seen in the Cu(1) BVS wave between 300 and 5 K. Although the average Cu(1) BVS value remains almost unchanged with temperature, the maximum (minimum) BVS value is much larger (smaller) in the wave at 300 K with larger amplitude. Indeed, the maximum value decreases from 2.33 to 2.23 with lowering temperature. This exactly reflects the increase in the minimum Cu(1)-O(3) distance at 5 K. On the other hand, the Cu(2) BVS waves have a larger amplitude than the Cu(1) waves, but their temperature dependence is small, in particular in the upper part of the wave.

Holes are expected to be located at the Cu sites having larger BVS values. Accordingly, most holes preferably occupy the Cu(2) sites, and the remaining holes do the Cu(1) sites with pyramidal coordination. Since the total number of holes in the system is constant, the decrease in the maximum Cu(1) BVS value suggests that the holes located in the ladder at 300 K tend to move into the chain with lowering tempera-

TABLE III. Refined lattice parameters for $\text{Sr}_{0.4}\text{Ca}_{13.6}\text{Cu}_{24+y}\text{O}_{41+z}$. Numbers in parentheses are estimated standard deviations of the last significant digit.

	5 K	300 K ^a
a (Å)	11.2565(2)	11.26078(1)
b (Å)	12.3820(2)	12.42666(2)
c_1 (Å)	3.90136(6)	3.904911(6)
c_2 (Å)	2.73607	2.73821
V_1 (Å ³)	543.761	546.429
V_2 (Å ³)	381.345	383.168
$k (= c_1/c_2)$	1.42590(6) (~77/54)	1.42608(1) (~164/115)
Chemical formula	$\text{Sr}_{0.4}\text{Ca}_{13.6}\text{Cu}_{23.981}\text{O}_{40.963}$ ($y = -0.019, z = -0.037$)	$\text{Sr}_{0.4}\text{Ca}_{13.6}\text{Cu}_{23.983}\text{O}_{40.965}$ ($y = -0.017, z = -0.035$)

^aFrom Ref. 12.

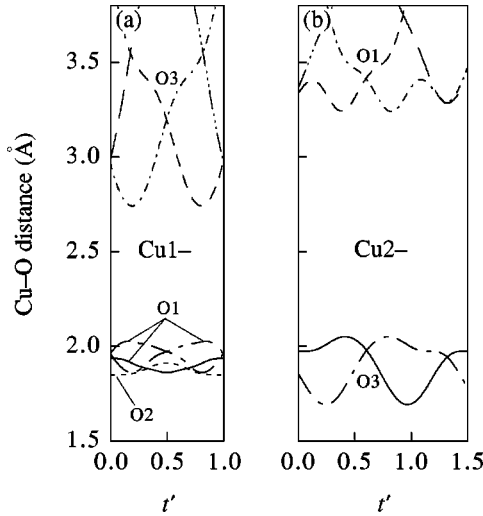


FIG. 4. Cu(1)-O (a) and Cu(2)-O (b) interatomic distances in $\text{Sr}_{0.4}\text{Ca}_{13.6}\text{Cu}_{23.981}\text{O}_{40.963}$ at 5 K plotted against a fourth coordinate t' . The average of the Cu(1)-O(3) distances is 2.877 Å, while the minimum is 2.740 Å.

ture. We estimated the number of holes remaining in the ladder at 5 K using an approximately commensurate supercell with a large c -dimension lattice parameter of $c = 54c_1 = 77c_2$ [$k = c_1/c_2 = 1.42590(6) \approx 77/54$ at 5 K] and a composition of $[(\text{Sr}_{0.029}\text{Ca}_{0.971})_2\text{Cu}_2\text{O}_3]_{54}[\text{CuO}_2]_{77}$. This supercell includes 46 ‘‘self-doped’’ holes. We found that only about 4% of the total holes, namely, 2 out of 46 holes, occupy Cu(1) sites at 5 K. On the other hand, this value increases to 20% at 300 K. The BVS estimation clearly supports the hole redistribution from the ladder to the chain with lowering temperature and indicates that almost all of the holes are localized in the chain at low temperature near or below T_N .

Very recently, it has been reported for $\text{Sr}_{14}\text{Cu}_{24}\text{O}_{41}$ that the spectral weight of optical conductivity shifts from a low- to a high-energy region with lowering temperature.²⁵ This finding gives evidence for a hole transfer from the ladder

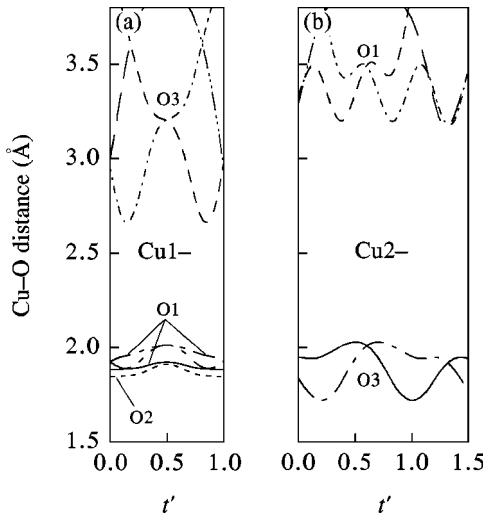


FIG. 5. Cu-O (a) and Cu(2)-O (b) interatomic distances in $\text{Sr}_{0.4}\text{Ca}_{13.6}\text{Cu}_{23.983}\text{O}_{40.965}$ at 300 K plotted against a fourth coordinate t' . The average of the Cu(1)-O(3) distances is 2.896 Å, while the minimum is 2.661 Å (Ref. 12).

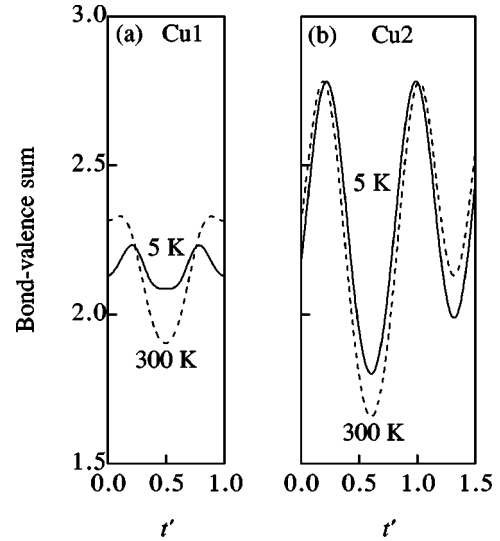


FIG. 6. Bond-valence sum waves of the Cu(1) (a) and Cu(2) (b) sites in $\text{Sr}_{0.4}\text{Ca}_{13.6}\text{Cu}_{24+y}\text{O}_{41+z}$ at 5 and 300 K plotted against the four-dimensional coordinate t' . Average values are 2.16 at 5 K and 2.16 at 300 K for the Cu(1) site, while 2.32 at 5 K and 2.30 at 300 K for the Cu(2) site.

into the chain and is consistent with our estimation. Optical measurements for highly Ca-doped samples are desired for further verification of the hole redistribution.

C. Magnetic structure in the antiferromagnetic state

The antiferromagnetic long-range order in this system mainly arises from the chain-Cu moment.⁴ Therefore, we focus here on only the chain plane, assuming that all holes are located there in the low-temperature region where the antiferromagnetism appears. In such a situation, the ladder-Cu moment vanishes owing to the formation of the spin singlet, without any contribution to the antiferromagnetism.

We start from consideration of the arrangement of the holes in the chain plane. Figure 7 shows the BVS values of

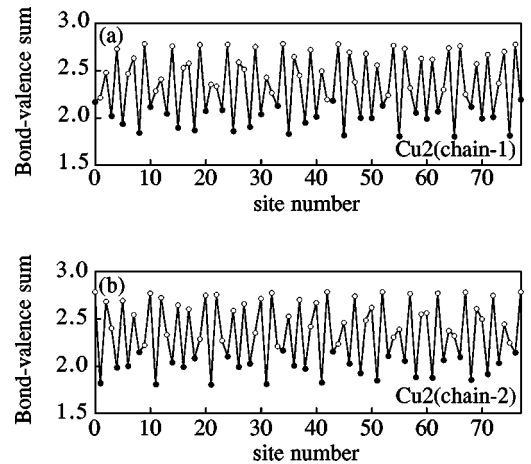


FIG. 7. Bond-valence sums of Cu(2) at 5 K along the two chains for the quasicommensurate supercell $[(\text{Sr}_{0.029}\text{Ca}_{0.971})_2\text{Cu}_2\text{O}_3]_{54}[\text{CuO}_2]_{77}$. The open circles indicate hole-occupied sites, while the solid circles indicate hole-unoccupied sites.

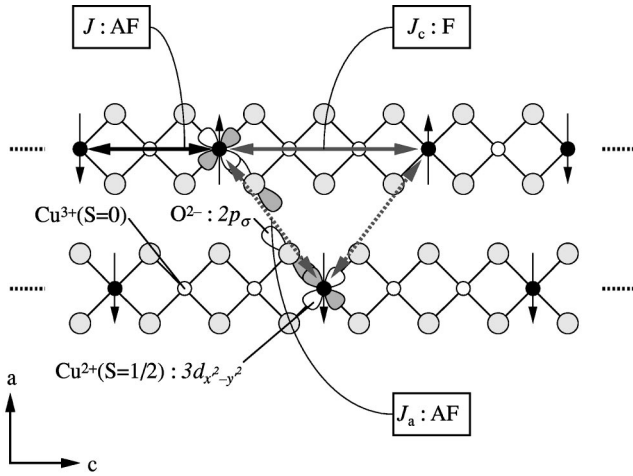


FIG. 8. Three major magnetic interactions J , J_c , and J_a , between Cu(2) spins on the a - c plane (indicated by bold arrows). The Cu(2) site with or without a hole is represented by small open or solid circle, respectively, and the Cu(2) spin is by an arrow. See text on the orbital configurations for the Cu-O-O-Cu quasilinear path.

Cu(2) at 5 K along the chain for the quasicommensurate supercell $[(\text{Sr}_{0.029}\text{Ca}_{0.971})_2\text{Cu}_2\text{O}_3]_{54}[\text{CuO}_2]_{77}$. In the commensurate three-dimensional description, the present system has two inequivalent chains corresponding to the x , y positions of the Cu(2) site in the unit cell: 0.25, 0.25 or 0.75, 0.75 (chain 1) and 0.75, 0.25 or 0.25, 0.75 (chain 2) (see Fig. 1). The open circles in Fig. 7 denote 46 hole-occupied sites having first to 46th large BVS values among the 77 Cu(2) sites, while the closed ones indicate hole-unoccupied sites. Holes occupy every other Cu(2) site in some part. However, two adjacent sites are also sometimes occupied successively, and the occupation sequence as a whole is complicated owing to the modulated structure. In Fig. 7 we did not find any evidence for a pinned charge-density wave that was reported for $\text{Sr}_{14}\text{Cu}_{24}\text{O}_{41}$.²⁶ Nevertheless, the arrangement of holes in Fig. 7 suggests a certain regularity and seems reasonable in view of the Coulomb repulsion between the charges. We have verified that the hole distribution determined by the BVS calculation is quite consistent with that obtained by calculating Madelung energies.²⁴

Cu^{2+} ions have $S=1/2$ spins, which correlate magnetically to one another. A doped hole strongly couples with a Cu^{2+} spin to form a Zhang-Rice (ZR) singlet, which can be regarded as a low-spin Cu^{3+} state ($S=0$: nonmagnetic). The hole-occupied Cu(2) sites in Fig. 7 can therefore be treated as nonmagnetic sites. According to the magnetic reflections observed for a single crystal, the antiferromagnetic spin direction is approximately parallel to the a axis.³ Based on this experimental result and the estimated hole distribution, we can construct a possible magnetic structure model for the antiferromagnetic state if we know effective magnetic interactions between the Cu(2) spins.

We considered three major interactions between the Cu(2) spins as shown in Fig. 8. The first one J is an interaction between the second-nearest-neighbor spins along the chain in a configuration of spin-hole-spin. We assumed that this term is antiferromagnetic and the main origin of the dimerized spin-singlet ground state in the chain. This assumption is based on neutron experiments and theoretical studies. Neu-

tron inelastic scattering measurements for $\text{Sr}_{14}\text{Cu}_{24}\text{O}_{41}$ confirmed the presence of spin dimers formed along the chain with a spin-spin correlation length as large as twice the Cu(2)-Cu(2) distance.²⁷ Its intradimer coupling is also estimated to be 10–11 meV.^{28,29} Matsuda *et al.*²⁹ have reported that the magnetic interactions are almost unchanged with Ca substitution for Sr. Furthermore, Mizuno *et al.*³⁰ theoretically predicted that the exchange interaction between the second-nearest-neighbor Cu ions in an edge-shearing Cu-O chain is antiferromagnetic in any ranges of structural and energy parameters.

The second one J_c is an interaction in the configuration of spin-hole-hole-spin between the third-nearest-neighbor spins along the chain via two hole-occupied sites (see Fig. 8). We assumed that this correlation is ferromagnetic with a much smaller exchange energy than J , i.e., $|J_c| \ll |J|$. Such an interaction has been observed as an interdimer spin correlation by neutron inelastic scattering measurements. Indeed, Regnault *et al.*²⁸ reported that an average interdimer distance along the chain is about 3 times longer than the Cu(2)-Cu(2) distance and that the spin correlation between the dimers is ferromagnetic with an exchange energy of ~ -1.1 meV. Their observation seems to support our assumption.

The third interaction J_a is an interchain coupling and acts between spins of adjacent chains through a quasistraight Cu-O-O-Cu path (see Fig. 8). We assumed that this term is antiferromagnetic on the basis of the orbital configurations for the Cu and O ions in the Cu-O-O-Cu path. The $3d_{x^2-y^2}$ orbital of the Cu ion strongly overlaps with the $2p_\sigma$ orbital of the O ion, and the two O $2p_\sigma$ orbitals would slightly overlap with each other. For such an arrangement of orbitals, spin hopping through the path is expected, resulting in an antiferromagnetic coupling due to the superexchange process. Regnault *et al.*²⁸ observed that the dimer-dimer spin correlation between the adjacent chains is antiferromagnetic with an exchange energy of ~ 1.7 meV. Their observation may reflect the interchain Cu-O-O-Cu interaction.

Based on the three magnetic interactions, we successfully constructed a magnetic structure model as illustrated in Fig. 9(a). The A and B planes are alternately stacked along the b axis as $\cdots(\text{A plane})-(\text{B plane})-(\text{A plane})\cdots$. It should be stressed that all the spins in Fig. 9(a) are arranged without spin frustration as regards the three interactions.

In order to test the proposed magnetic structure model, we calculated the magnetic structure factors for the supercell $[(\text{Sr}_{0.029}\text{Ca}_{0.971})_2\text{Cu}_2\text{O}_3]_{54}[\text{CuO}_2]_{77}$ using a Rietveld-analysis program RIETAN-98,³¹ with the crystal data obtained in the present study. In the calculation, we assumed that all magnetic moments are parallel to the a axis with a constant effective Bohr magneton of $0.3\mu_B$, which was estimated from static magnetic measurements.¹³ Figure 10 shows the square of magnetic structure factors calculated for $(10l)$, $(01l)$, and $(h054)$ sections, where the index l is based on the $c=77c_2$ cell. Nagata *et al.*³ measured the magnetic reflections for a single crystal and analyzed them using a $c=17c_2$ supercell. For the $(10l)$ section, they observed a strong $10\bar{1}2$ and a weak $102\bar{2}$ reflection. These indices correspond to 1010 and $10\bar{1}2$ in the four-dimensional description and coincide with 1054 and $10\bar{1}00$ in the present $77c_2$ cell, respectively. [Note that the upper lateral axis in Fig. 10(a) is scaled to the c

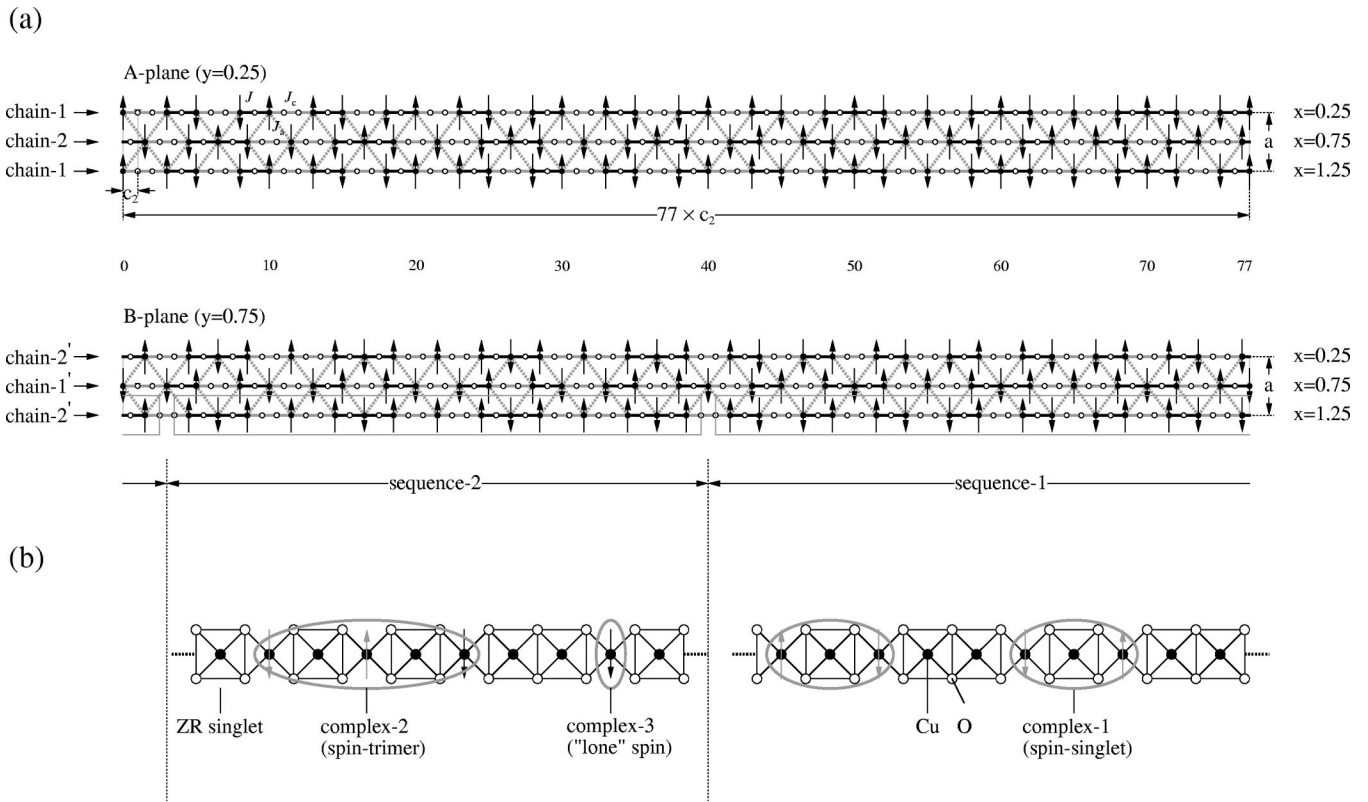


FIG. 9. (a) A possible magnetic structure model for Cu(2) spins in the chain plane for the quasicommensurate supercell $[(\text{Sr}_{0.029}\text{Ca}_{0.971})_2\text{Cu}_2\text{O}_3]_{54}[\text{CuO}_2]_{77}$ (the O atoms are omitted). The three major magnetic interactions are represented by solid lines (J), gray lines (J_c), and gray dotted lines (J_a). (b) Two types of sequences in a chain, in which three kinds of magnetic complexes are formed by the spin and Zhang-Rice singlet (see text).

$=17c_2$ cell.] Our calculation qualitatively reproduces the observed reflections. For the $(01l)$ and $(h054)$ sections, the calculated reflections also agree well with the experimental results at least in terms of the peak positions. Some relative intensities in the calculated results are different from those in the observed ones by a factor of ~ 2 maximum. The main reason for the difference is probably that we have taken no account of the staggered spin modulation of the magnetic moment.^{9,10} This point is discussed later in brief.

Furthermore, we simulated a neutron powder diffraction pattern using RIETAN-98, including magnetic scattering as well as nuclear one. Such a simulation is helpful to know the relative contribution of the magnetic scattering to the total pattern. The resulting pattern is shown in Fig. 11(a). The 0123 reflection has the maximum intensity of purely magnetic reflections. However, it is extremely weak as compared with other reflections due to mainly nuclear scattering. Using the HERMES diffractometer, we measured neutron powder diffraction patterns above and below T_N and obtained a difference pattern between them as shown in Fig. 11(b). No peak was detected clearly near $2\theta \approx 14^\circ$, i.e., the position of the 0123 reflection. This experimental fact supports the present simulation result at least in terms that the magnetic contribution to the neutron powder pattern is minimal.

We found that the reasonable magnetic structure model is comprised of the three magnetic interactions illustrated in Fig. 8. If we consider the J term as the most principal interaction, we can extract three kinds of complexes of the spin and the ZR singlet from each chain [see Fig. 9(b)]. Using

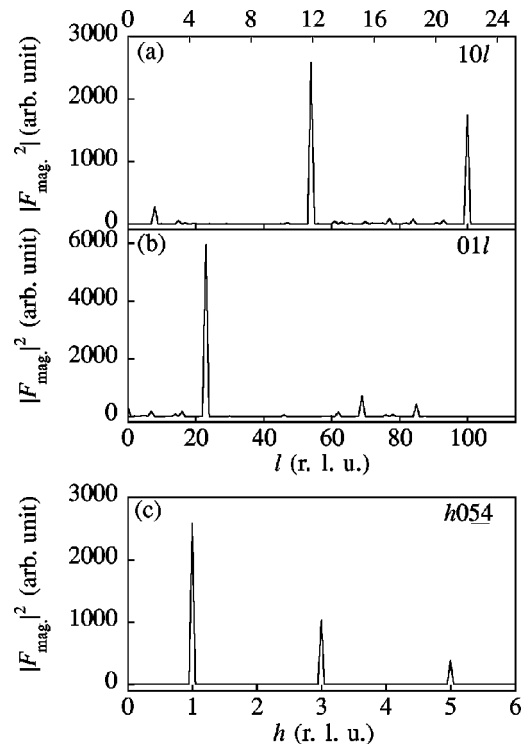


FIG. 10. Square of magnetic structure factors in $(10l)$, $(01l)$, and $(h054)$ sections calculated for the quasicommensurate supercell $[(\text{Sr}_{0.029}\text{Ca}_{0.971})_2\text{Cu}_2\text{O}_3]_{54}[\text{CuO}_2]_{77}$. The upper lateral axis in (a) is scaled to the $c = 17c_2$ cell (see text).

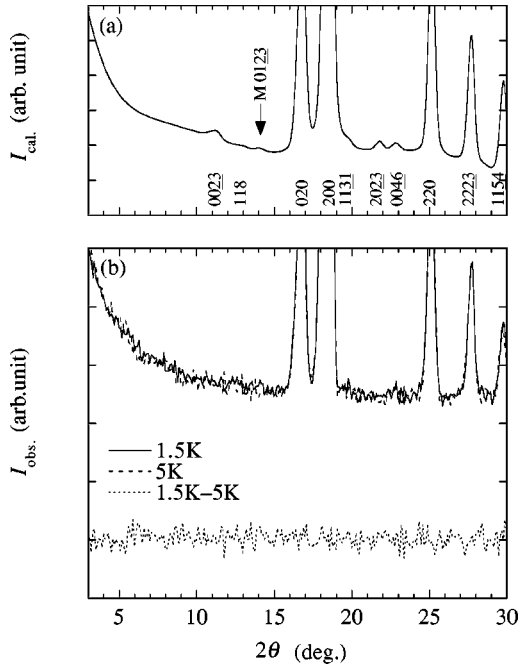


FIG. 11. Neutron powder diffraction patterns for $\text{Sr}_{0.4}\text{Ca}_{13.6}\text{Cu}_{24+y}\text{O}_{41+z}$: (a) Simulated pattern for the quasicommensurate supercell $[(\text{Sr}_{0.029}\text{Ca}_{0.971})_2\text{Cu}_2\text{O}_3]_{54}[\text{CuO}_2]_{77}$. (b) Experimental patterns observed at 1.5 and 5 K, and their difference pattern.

simple notations $+$, $-$, and 0 for an up-spin, a down-spin, and a ZR singlet, respectively, the first complex is represented by $\langle +0- \rangle$ (or $\langle -0+ \rangle$). This complex apparently corresponds to a spin dimer observed in inelastic neutron scattering studies.^{27–29} The second is $\langle +0-0+ \rangle$ (or $\langle -0+0- \rangle$). This complex seems to be regarded as a kind of spin trimer that consists of a spin singlet and a spin. The third is just $\langle + \rangle$ (or $\langle - \rangle$), namely, a “lone” spin. These complexes are separated from one another along the chain by two adjoining ZR singlets (an “extended ZR singlet”³²) 00 and weakly interact through J_c and J_a .

Two types of sequences on these complexes are seen in each chain. One consists of only the first complexes, such as $\cdots 00 \langle +0- \rangle 00 \langle -0+ \rangle 00 \langle +0- \rangle 00 \langle -0+ \rangle 00 \cdots$. The NMR and nuclear quadrupole resonance (NQR)³² and neutron inelastic scattering experiments^{28,29} support the presence of this sequence. The other sequence consists of an alternation of the second complexes and “lone” spins such as $\cdots 00 \langle -0+0- \rangle 00 \langle - \rangle 00 \langle -0+0- \rangle 00 \langle - \rangle 00 \langle -0+0- \rangle 00 \cdots$ for the A plane and $\cdots 00 \langle +0-0+ \rangle 00 \langle + \rangle 00 \langle +0-0+ \rangle 00 \langle + \rangle 00 \langle +0-0+ \rangle 00 \cdots$ for the B plane. This sequence is proposed and may be important for understanding the occurrence of antiferromagnetic long-range order.

According to the theory,^{9,10} the effective magnetic moment on the spin singlet exponentially decays as it recedes from the lone spin that is created by the hole or impurity doping, and the spin-singlet nonmagnetic state becomes dominant at a place far away from the spin. Although we did not take it into account in the aforementioned procedure, such nonuniformity of the magnetic moment on the chain has been pointed out by NMR & NQR studies.⁴ As an extreme case of this picture, we can neglect all the magnetic moments except for that of the spin in question. In our magnetic struc-

ture model, the “lone” spin ($\langle + \rangle$ or $\langle - \rangle$) and the “spin trimer” ($\langle +0-0+ \rangle$ or $\langle -0+0- \rangle$) may be replaced by an $S=1/2$ spin each, and the magnetic moment in the “spin dimer” ($\langle +0- \rangle$ or $\langle -0+ \rangle$) may be ignored. The resultant model corresponds to the extreme case. According to this model, the number of the $S=1/2$ spins surviving becomes a few percent of the total $\text{Cu}(2)$ sites. In a previous study of the static magnetic moment, we have obtained a similar value to the number of spins on the assumption of the $S=1/2$ spin state.¹³ The real situation would be intermediate between the two extreme cases, i.e., the uniform model and the model based on the $S=1/2$ spin. To obtain a more sophisticated magnetic structure model, we need to analyze the magnetic reflections in the four-dimensional space, although such a method has not been developed as yet.

V. SUMMARY

The hole distribution and magnetic structure in the antiferromagnetic long-range-ordered state in $\text{Sr}_{0.4}\text{Ca}_{13.6}\text{Cu}_{24+y}\text{O}_{41+z}$ have been studied by a detailed analysis of the low-temperature crystal structure using neutron diffraction data with a technique on the basis of a four-dimensional description of the modulated structure. As a result, we drew the two following conclusions, which are important to understand the low-temperature properties of this material. The first conclusion is that as the temperature is lowered the holes are redistributed from the ladder to the chain. The BVS calculation suggests that almost all of the holes are located in the chain below or near T_N and ordered there with regularity due to the modulated structure. The second conclusion is that an unusual magnetic structure exists in the antiferromagnetic phase, which can describe the coexisting state of the long-range order and spin singlets in the chain. The magnetic state includes three kinds of magnetic complexes of spin dimers, spin trimers, and “lone” spins in the chain. The latter two have effective magnetic moments, which may be the origin of staggered antiferromagnetic spin modulation induced onto the spin singlets. These conclusions suggest that the antiferromagnetic long-range order in this system is ascribed to the charge order in the chain.

ACKNOWLEDGMENTS

We would like to thank Y. Matsui (NIRIM) for helpful advice in the electron microscopy, A. Yamamoto (NIRIM) for modification of the analysis program, and Y. Uchida (NIRIM) for his numerous and stimulating discussions on magnetism. One of the authors (M.I.) is deeply grateful to K. Kakurai and M. Nishi of The University of Tokyo for encouraging the neutron diffraction experiments at JAERI and for enlightening discussions on the magnetic structure, as well as to K. Nemoto (Tohoku University) and Y. Kanke (NIRIM) for their help on the neutron diffraction experiments. This work was supported by the Multi-Core Project organized by the Science and Technology Agency of Japan.

- ¹N. Motoyama, T. Osafune, T. Kakeshita, H. Eisaki, and S. Uchida, *Phys. Rev. B* **55**, R3386 (1997).
- ²T. Osafune, N. Motoyama, H. Eisaki, and S. Uchida, *Phys. Rev. Lett.* **82**, 1313 (1999).
- ³T. Nagata, H. Fujino, J. Akimitsu, M. Nishi, K. Kakurai, S. Katanano, M. Hiroi, M. Sera, and N. Kobayashi, *J. Phys. Soc. Jpn.* **68**, 2206 (1999).
- ⁴S. Ohsugi, K. Magishi, S. Matsumoto, Y. Kitaoka, T. Nagata, and J. Akimitsu, *Phys. Rev. Lett.* **82**, 4715 (1999).
- ⁵T. Osafune, N. Motoyama, H. Eisaki, and S. Uchida, *Phys. Rev. Lett.* **78**, 1980 (1996).
- ⁶M. Kato, K. Shiota, and Y. Koike, *Physica C* **258**, 284 (1996).
- ⁷M. Isobe, T. Ohta, M. Onoda, F. Izumi, S. Nakano, J. Q. Li, Y. Matsui, E. Takayama-Muromachi, M. Matsumoto, and H. Hayakawa, *Phys. Rev. B* **57**, 613 (1998).
- ⁸M. Uehara, T. Nagata, J. Akimitsu, H. Takahashi, N. Mori, and K. Kinoshita, *J. Phys. Soc. Jpn.* **65**, 2764 (1996).
- ⁹H. Fukuyama, T. Tanimoto, and M. Saito, *J. Phys. Soc. Jpn.* **65**, 1182 (1996).
- ¹⁰H. Fukuyama, N. Nagaosa, M. Saito, and T. Tanimoto, *J. Phys. Soc. Jpn.* **65**, 2377 (1996).
- ¹¹I. D. Brown and D. Altermatt, *Acta Crystallogr., Sect. B: Struct. Sci.* **41**, 244 (1985).
- ¹²T. Ohta, F. Izumi, M. Onoda, M. Isobe, E. Takayama-Muromachi, and A. W. Hewat, *J. Phys. Soc. Jpn.* **66**, 3107 (1997).
- ¹³M. Isobe, Y. Uchida, and E. Takayama-Muromachi, *Phys. Rev. B* **59**, 8703 (1999).
- ¹⁴A. W. Hewat, *Mater. Sci. Forum* **9**, 69 (1986).
- ¹⁵K. Ohoyama, T. Kanouchi, K. Nemoto, M. Ohashi, T. Kajitani, and Y. Yamaguchi, *Jpn. J. Appl. Phys., Part 1* **37**, 3319 (1998).
- ¹⁶Y. Matsui, S. Horiuchi, Y. Bando, Y. Kitami, M. Yokoyama, S. Suehara, I. Matsui, and T. Katsuta, *Ultramicroscopy* **39**, 8 (1991).
- ¹⁷E. M. McCarron III, M. A. Subramanian, J. C. Calabrese, and R. L. Harlow, *Mater. Res. Bull.* **23**, 1355 (1988).
- ¹⁸A. Yamamoto, *Acta Crystallogr., Sect. A: Cryst. Phys., Diffr., Theor. Gen. Crystallogr.* **38**, 87 (1982).
- ¹⁹T. Janssen, A. Janner, A. Looijenga-Vos, and P. M. de Wolff, in *International Tables for Crystallography*, edited by A. J. C. Wilson (Kluwer, Dordrecht, 1992), Vol. C, p. 797.
- ²⁰A. Yamamoto, *Acta Crystallogr., Sect. A: Found. Crystallogr.* **49**, 831 (1993); **52**, 509 (1996).
- ²¹*International Tables for Crystallography* (Ref. 19), Vol. C, pp. 384 and 500.
- ²²M. Onoda, *J. Crystallogr. Soc. Jpn.* **40**, 161 (1998); **40**, 202 (1998).
- ²³P. M. de Wolff, *Acta Crystallogr., Sect. A: Cryst. Phys., Diffr., Theor. Gen. Crystallogr.* **30**, 777 (1974).
- ²⁴M. Isobe and E. Takayama-Muromachi, *J. Phys. Soc. Jpn.* **67**, 3119 (1998).
- ²⁵M. Someya, K. Kojima, H. Eisaki, and S. Uchida, in *Meeting Abstracts of the Physical Society of Japan*, edited by The Physical Society of Japan (Nihon-Butsuri-Gakkai, Tokyo, 1999), Vol. 54, Issue 2, Pt. 3, p. 435.
- ²⁶D. E. Cox, T. Iglesias, K. Hirota, G. Shirane, M. Matsuda, N. Motoyama, H. Eisaki, and S. Uchida, *Phys. Rev. B* **57**, 10 750 (1998).
- ²⁷M. Matsuda, K. Katsumata, H. Eisaki, N. Motoyama, and S. Uchida, *Phys. Rev. B* **54**, 12 199 (1996).
- ²⁸L. P. Regnault, J. P. Boucher, H. Moudden, J. E. Lorenzo, A. Hiess, U. Ammerahl, G. Dhalenne, and A. Revcolevschi, *Phys. Rev. B* **59**, 1055 (1999).
- ²⁹M. Matsuda, T. Yoshihama, K. Kakurai, and G. Shirane, *Phys. Rev. B* **59**, 1060 (1999).
- ³⁰Y. Mizuno, T. Tohyama, S. Maekawa, T. Osafune, N. Motoyama, H. Eisaki, and S. Uchida, *Phys. Rev. B* **57**, 5326 (1998).
- ³¹F. Izumi, in *The Rietveld Method*, edited by R. A. Young (Oxford University Press, Oxford, 1993), Chap. 13; in *Applications of Synchrotron Radiation to Materials Analysis*, edited by H. Saisho and Y. Gohshi (Elsevier Science, Amsterdam, 1995), Chap. 7.
- ³²M. Takigawa, N. Motoyama, H. Eisaki, and S. Uchida, *Phys. Rev. B* **57**, 1124 (1998).